THEORY VERSUS EXPERIMENT FOR THE ROTORDYNAMIC[1] COEFFICIENTS OF ANNULAR GAS SEALS: PART 2, CONSTANT-CLEARANCE AND CONVERGENT-TAPERED GEOMETRY

Clayton C. Nelson, Assistant Professor
Dara W. Childs, Professor
Colby Nicks, Research Assistant[2]
David Elrod, Research Assistant

Mechanical Engineering Department
Turbomachinery Laboratories
Texas A&M University
College Station, Texas 77843

ABSTRACT

An experimental test facility is used to measure the leakage and rotordynamic coefficients of constant-clearance and convergent-tapered annular gas seals. The results are presented along with the theoretically predicted values. Of particular interest is the prediction that optimally tapered seals will have significantly larger direct stiffness than straight seals. The experimental results verify this prediction. Generally the theory does quite well, but fails to predict the large increase in direct stiffness when the fluid is prerotated.

[1]This work was supported in part by NASA Grant NAS8-33716 from NASA Lewis Research Center (Technical Monitor, Robert Hendricks) and AFOSR Contract F49620-82-k-0033 (Technical Monitor, Tony Amos).

[2]Currently employed at Bell Helicopter, Fort Worth, Texas.

NOMENCLATURE

A = cross-sectional flow area of the seal (L^2)

C_r = seal clearance (L)

C,c = direct and cross-coupled damping coefficients (FT/L)

F = reaction force (F)

f = Darcy friction factor

K,k = direct and cross-coupled stiffness coefficients (F/L)

k_l = loss coefficient

M = Mach number

$\dot{m}$ = mass flow rate (M/T)

mo,no = Hirs' constants

p = pressure (F/L^2)

R = shaft radius (L)

$\bar{R}$ = Reynolds number, $2\rho V_m C_r/\mu$

R_g = perfect gas constant ($L^2/T^2\Theta$)

U_Z, U_θ = fluid velocity in the Z and θ direction (L/T)

V_m = bulk-flow velocity of the fluid (L/T)

γ = specific heat rato

μ = viscosity (FT/L^2)

ρ = density (M/L^3)

τ = shear stress (F/L^2)

ω = shaft angular velocity (T^{-1})

Subscripts

a,b = reservoir and sump

s,t = straight and tapered

X,Y,Z = rectangular coordinate directions

INTRODUCTION

Part 1 of this paper described the design, development, and operation of a test apparatus and facility which have been developed to measure leakage and rotordynamic coefficients of annular gas seals. This test apparatus has been designed and used to measure rotordynamic coefficients of plain annular seals (as used in floating-ring seals), plain seals with honeycomb stators, and labyrinth seals. This part (Part 2) of the paper provides a comparison of test results and theory for plain annular seals having constant-clearance and convergent-tapered geometries. Subsequent publications will provide test results for honeycomb and labyrinth seals.

As described in Part 1, the rotordynamic coefficients for a gas seal are defined by the following linearized force-displacement model.

$$-\begin{Bmatrix} F_X \\ F_Y \end{Bmatrix} = \begin{bmatrix} K_{XX} & K_{XY} \\ K_{YX} & K_{YY} \end{bmatrix} \begin{Bmatrix} X \\ Y \end{Bmatrix} + \begin{bmatrix} C_{XX} & C_{XY} \\ C_{YX} & C_{YY} \end{bmatrix} \begin{Bmatrix} \dot{X} \\ \dot{Y} \end{Bmatrix} \qquad (1)$$

Where (X, Y) define the relative motion of the seal rotor relative to its stator, (F_X, F_Y) are the components of the reaction force acting on the rotor, and $(K_{XX}, K_{YY}, K_{XY}, K_{YX})$ and $(C_{XX}, C_{YY}, C_{XY}, C_{YX})$ are the stiffness and damping coefficients respectively. Equation (1) applies for small motion of the rotor about an arbitrary eccentricity position. For small motion about a centered position, the following simpler model applies.

$$-\begin{Bmatrix} F_X \\ F_Y \end{Bmatrix} = \begin{bmatrix} K & k \\ -k & K \end{bmatrix} \begin{Bmatrix} X \\ Y \end{Bmatrix} + \begin{bmatrix} C & c \\ -c & C \end{bmatrix} \begin{Bmatrix} \dot{X} \\ \dot{Y} \end{Bmatrix} \qquad (2)$$

Although the test facility has the capability of measuring the eccentric-position rotordynamic coefficients of Eq. (1), present analytical solutions are only capable of predicting the centered-position coefficients of Eq. (2). Thus, all test results reported in this paper will be for the shaft-centered position.

Analytical Developments

Literature pertaining to the analytical solution for the rotordynamic coefficients of annular gas-path seals is extremely limited. Fleming [1,2] analyzed convergent-tapered gas seals using a seperate analysis to determine the direct stiffness K and the direct damping C. His analysis concludes that optimally tapered seals will develop considerably higher direct stiffness than straight seals. However, since his analysis does not include fluid prerotation (preswirl) he was not able to predict the cross-coupled coefficients c and k. Recently Nelson [3,4] developed an analytical-computational method to solve for all of the rotordynamic coefficients in Eq. 2. His solution technique is similar to that developed by Childs [5,6]. That is, a set of governing equations based on Hir's [7] turbulent bulk flow model are developed, and then a perturbation analysis is employed to obtain a set of zero- and first-order equations. Integration of the zeroth-order equations yields the leakage, and integration of the first-order equations yields the direct and cross-coupled rotordynamic coefficients. The analysis handles choked or unchoked flow, the effect of different stator and rotor

surface roughness conditions, and straight or tapered seal geometries. His solution agrees with Fleming's prediction that convergent-tapered seals develop higher direct stiffnesses. The test results presented in this paper are compared with the theoretical predictions of Nelson's solution.

TEST VARIABLES

There are fifteen independent input variables required for the theoretical solution of the smooth, convergent-tapered, annular gas seal. These values can be grouped into the three categories: geometry, gas properties, and operating conditions. The values (or range of values) used for the theoretical solution are shown in Table I below. Following the table is a description of how these values were obtained from the test apparatus.

Geometry	
length:	8 cm (2.00 in)
diameter:	24 cm (6.00 in)
entrance clearance:	0.7366 mm (29 mil)
exit clearance:	0.7366 mm (29 mil) (straight) 1.1143 mm (45 mil) (tapered)
Hir's constants:	no = 0.187 mo = -0.333
Gas Properties	
viscosity:	1.9×10^{-5} N•s/m^2 (4.0×10-7 lb•s/ft^2)
gas constant:	287 m•N/kg•K (53.3 ft•lb/lb$_m$•^{o}R)
specific heat ratio:	1.4
Operating Conditions	
reservoir pressure:	1.7 to 7.2 bar (25 - 104 psi)
reservoir temp:	305 K (90 ^{o}F)
sump pressure:	1.0 bar (14.7 psi)
preswirl ratio, $U_{\theta 0}(0)/R\omega$:	-81 to +81
shaft speed:	200 to 8000 cpm
precessional speed:	0.98 and 1.24 cpm

Table I. Values of the Independent Input Variables

Geometry. Figure 1 shows a simplified cross-sectional view of the rotor and stator. Both the stator and rotor are fabricated from 304 stainless steel with a 4 μin finish. The seal's length, diameter, and clearances are obtained from the given dimensions.

The theoretical solution is based on Hirs' turbulent bulk-flow model. That is, in the relationship for the wall shear stress,

$$\tau = (1/2)\rho V_m^2 f \tag{3}$$

it is assumed that the Fanning friction factor, f, is a variable according to the following relationship:

$$f = no(\bar{R})^{mo} \tag{4}$$

In these equations, V_m is the mean bulk-flow velocity and $\bar{R}$ is the Reynolds number, both relative to the surface upon which the shear stress is acting. The Hirs' coefficients no and mo account for the surface roughness and must be empirically determined. To determine the Hirs' constants for the test aparatus, static tests (i.e. no shaking nor rotation of the rotor) were run with the constant-clearance seal at several different reservoir pressure levels. The data collected from these tests included the mass flow rate, $\dot{m}$, reservoir temperature, Ta, reservoir pressure, pa, and the pressures at five axial locations. From these values, the Reynolds number is calculated, and the Mach number, M, is determined at each of the five axial locations from the following equation.

$$\dot{m} = \frac{pAM}{\sqrt{R_g T_a}} \left\{ \gamma \left[1 + \frac{(\gamma-1)}{2} M^2 \right] \right\}^{1/2} \tag{5}$$

These mach numbers were then used to solve for the left-hand side of the standard equation for choked, adiabatic, compressible flow in a duct with friction.

$$\frac{2fL^*_m}{C} = \frac{1-M^2}{\gamma M^2} + \frac{(\gamma+1)}{2\gamma} \ln\left\{\frac{(\gamma+1)M^2}{2\left[1 + \frac{(\gamma-1)M^2}{2}\right]}\right\} \qquad (6)$$

Here, L^*_m is the length of seal from the axial location m to the exit which would be necessary to produce choked flow. The average friction factor between any two arbitrary locations m and n can then be found from

$$f = \frac{C}{2L_{m,n}}\left(\frac{2fL^*_m}{C} + \frac{2fL^*_n}{C}\right) \qquad (7)$$

Subscript

where $L_{m,n}$ is the distance between points m and n. The mean friction factor was then found by averaging the results of different point combinations. Finally, the Hirs' constants, no and mo, were evaluated from a power law curve fit of the mean friction factors and the Reynolds number obtained at the various reservoir pressure levels.

Gas Properties: The fluid passing through the seal was air. The gas properties used were taken from standard tables.

Operating Conditions: To determine the effect of fluid prerotation (preswirl), the test rig design allows for the installation of a set of inlet vanes which accelerates the flow in the circumferential and axial direction. For tests in which there was no prerotation, no guide vanes were installed. With no vanes, the inlet cross-sectional area is significantly larger that the sealed area, and thus the measured inlet pressure and temperature is essentially equal to stagnation (reservoir) pressure and

temperature, and these values were used directly in the theoretical solution. For the case in which the guide vanes were installed, appropriate corrections were made to the accelerated flow to convert the measured values back to the reservoir conditions.

The preswirl ratio, $U(0)/R\omega$, is the ratio of the entering fluid's circumferential velocity to the surface speed of the shaft. Although the inlet guide vane angle is fixed, this ratio varies as the pressure drop across the seal and the shaft speed is changed. For the largest pressure drop and the slowest shaft speed, the ratio has a value of $\cong \pm 81$. The plus sign indicates flow which has been prerotated in the direction of shaft rotation, and the negative sign indicates prerotation against. For the smallest pressure drop and the fasted shaft speed, the ratio has a value of $\cong \pm 1.8$.

The theoretical model assumes that the shaft precesses in a small elliptical orbit about the shaft-centered position. In the test apparatus, the shaft is shaken horizontally about the centered position. The shake frequencies used were 58.8 and 74.4 Hertz (0.98 and 1.24 cpm). Text results were essentially the same for both these frequencies.

TEST RESULTS

Figure 2 shows the axial pressure gradient for the static test of the constant-clearance seal. The upper plot is for non-prerotated fluid, and the lower plot is for prerotated fluid in which the prerotation opposes the rotor rotation. The solid line is for the measured values, and the dashed line represents theory. For non-prerotation, agreement between theory and experiment is excellent. This is to be expected, however, since the Hirs' coefficients used in the analysis come directly from the measured pressures. For the prerotated case, the agreement is not as good. As stated earlier, when the inlet guide vanes are installed, appropriate corrections are made to the accelerated flow to convert the measured inlet flow conditions back to their reservoir conditions. Since the experimental plot shows the measured static pressure (not yet corrected to reservoir conditions), there is naturally a difference between theory and experiment at the front of the seal entrance. Just after the seal entrance, however, theory and experiment should agree. The sudden drop in the pressure at the entrance is due to conversion of pressure energy to kinetic energy and due to non-isentropic losses. The non-isentropic losses are accounted for in the theoretical solution by a loss coefficient which is approximated from the data of Deissler [8] as

$$k_1 = \sqrt{5.3/\log_{10} \bar{R}} - 1.0 \qquad (8)$$

From the lower plot in Fig. 2, it appears that this coefficient underestimates the entrance losses when the fluid is prerotated with the inlet guide vanes. This same general result is seen for prerotation in either direction, and for both the constant-clearance and convergent-tapered seal.

Experimental data was taken at shaft rotor speeds of 200, 500, and 1000-8000 rpm, in 1000 rpm increments. Figure 3 shows the direct stiffness, Kxx, vs. these rotor speeds for a fixed pressure ratio (pa/pb). It can be seen that there is very little dependence on rotor speed. This result is typical for all the rotordynamic coefficients and leakage at any of the pressure ratios tested and for both the constant-clearance and convergent tapered seal.

Figures (4-8) shows the measured and predicted leakage and rotordynamic coefficients vs. pressure ratio. In each figure, the upper plot is for the constant-clearance seal and the lower plot is for the convergent-tapered seal. Each plot shows the results for three cases: (1) no fluid prerotation, (2) fluid prerotated in the direction of the shaft rotation, and (3) fluid prerotated against the direction of the shaft rotation. Since there was little dependence of the leakage and rotordynamic coefficients on shaft speed over the range tested, average values measured over the speed range were used as the data points on the plots, with a vertical line at each point indicating the variance. The predicted values are shown by the solid line.

Predicted and measured values for the leakage of the straight and tapered seal are shown in Fig. 4. The agreement is excellent. Figure 5 shows the direct stiffness. The most notable result in this figure is the effect that prerotation of the fluid has on the

experimentally measured values of K. Prerotating the fluid causes a two- to three-fold increase. However, the theoretical solution does not account for this effect. The predicted values are all within the range of the measured values, but essentially indicates very little effect of prerotation.

Figure 6 shows the cross-coupled stiffness. Agreement between the predicted values and the measured values is fairly good. For no prerotation, both measured and predicted are nominally zero. For the prerotated, the predicted values run 0 - 40% larger than measured.

Figure 7 shows the direct damping. For the straight seal the agreement between theory and experiment is excellent. For the tapered seal the theory runs 0 - 30% smaller than measured.

Figure 8 show the cross-coupled damping. Again, for no prerotation, both measured and predicted values are nominally zero. However, the theory significantly underestimates c for most of the prerotated cases.

DISCUSSION

As stated in the introduction, both Fleming's [2,3] and Nelson's [4,5] analytical solution predicts that an optimally tapered seal will develop considerably higher direct stiffness than straight seals. The experimental results verifies this prediction. This can more easily be seen in Fig. 9. In this plot the vertical axis represents the ratio of the direct stiffness for the tapered seal to the direct stiffness of the constant-clearance seal. The theory predicts stiffness ratios of 1.3 to 2.0 as the pressure ratio is increased, and is essentially not influenced by fluid prerotation. The measured results show ratios of 1.2 to 1.5 and 1.6 to 2.3 for prerotated fluid, and ratios of 1.6 to 2.7 for no prerotation.

Generally the theory appears to work quite well. It does an excellent job of predicting the leakage and the direct damping, and does a fairly good job of predicting the cross-coupled stiffness. The most notable failure is in accounting for the effect of fluid prerotation on the direct stiffness. As previously noted, the empirical model of Deissler's [9] used for the inlet losses in the theoretical solution is not adequate when the inlet guide vanes are installed. Improved modeling of the inlet losses may improve the accuracy of the stiffness predictions.

Finally, agreement between experiment and theory for the cross-coupled damping coefficient is at best marginal. However, the actual force produced by the effect of c is much smaller than the other rotordynamic coefficients. Thus, its effect on rotordynamic calculations is rather insignificant.

REFERENCES

1. Fleming, D. P., "Stiffness of Straight and Tapered Annular Gas Path Seals," ASME J. Lub. Tech., Vol. 101, No. 3, July 1979, pp. 349-355.

2. Fleming, D. P., "Damping in Ring Seals for Compressible Fluids," NASA CP2133, Rotordynamic Instability Problems in High-Performacne Turbomachinery, proceedings of a workshop held at Texas A&M University, May 12-14 1980, pp. 169-188.

3. Nelson, C. C., "Rotordynamic Coefficients for Compressible Flow in Tapered Annular Seals," Accepted for publication in the ASME Journal of Tribology.

4. Nelson, C. C., "Analysis for Leakage and Rotordynamic Coefficients of Surface Roughened Tapered Annular Gas Seals," ASME Trans. J. Engineering for Power, October 1984, pp 927-934.

5. Childs, D. W., "Dynamic Analyusis of Turbulent Annular Seals Based on Hirs' Lubrication Equations," ASME Trans., J. of Lub. Tech., Vol. 105, July 1983, pp 429-436.

6. Childs, D. W., "Finite-Length Solutions for the Rotordynamic Coefficients Turbulent Annular Seals," ASME Trans., J. of Lub. Tech., Vol. 105, July 1983, pp 437-444.

7. Hirs, G. G., "A Bulk-Flow Theory for Turbulence in Lubricant Films," ASME J. of Lub. Tech., Apr. 1973, pp. 137-146.

8. Deissler, R. G., "Analysis of Turbulent Hear Transfer and Flow in the Entrance Regions of Smooth APassages," NACA TN 3016, 1953.

LIST OF FIGURES

page

Figure 1. Cross-sectional view of the seal test section.

Figure 2. Axial pressure gradient for the static test of the constant-clearance seal.

Figure 3. Direct stiffness vs. rotor speed for the constant-clearance seal.

Figure 4. Leakage vs. pressure ratio for the straight and tapered seal.

Figure 5. Direct stiffness vs. pressure ratio for the straight and tapered seal.

Figure 6. Cross-coupled stiffness vs. pressure ratio for the straight and tapered seal.

Figure 7. Direct damping vs. pressure ratio for the straight and tapered seal.

Figure 8. Cross-coupled damping vs. pressure ratio for the straight and tapered seal.

Figure 9. Direct Stiffness ratio of the straight and tapered seal vs. pressure ratio.

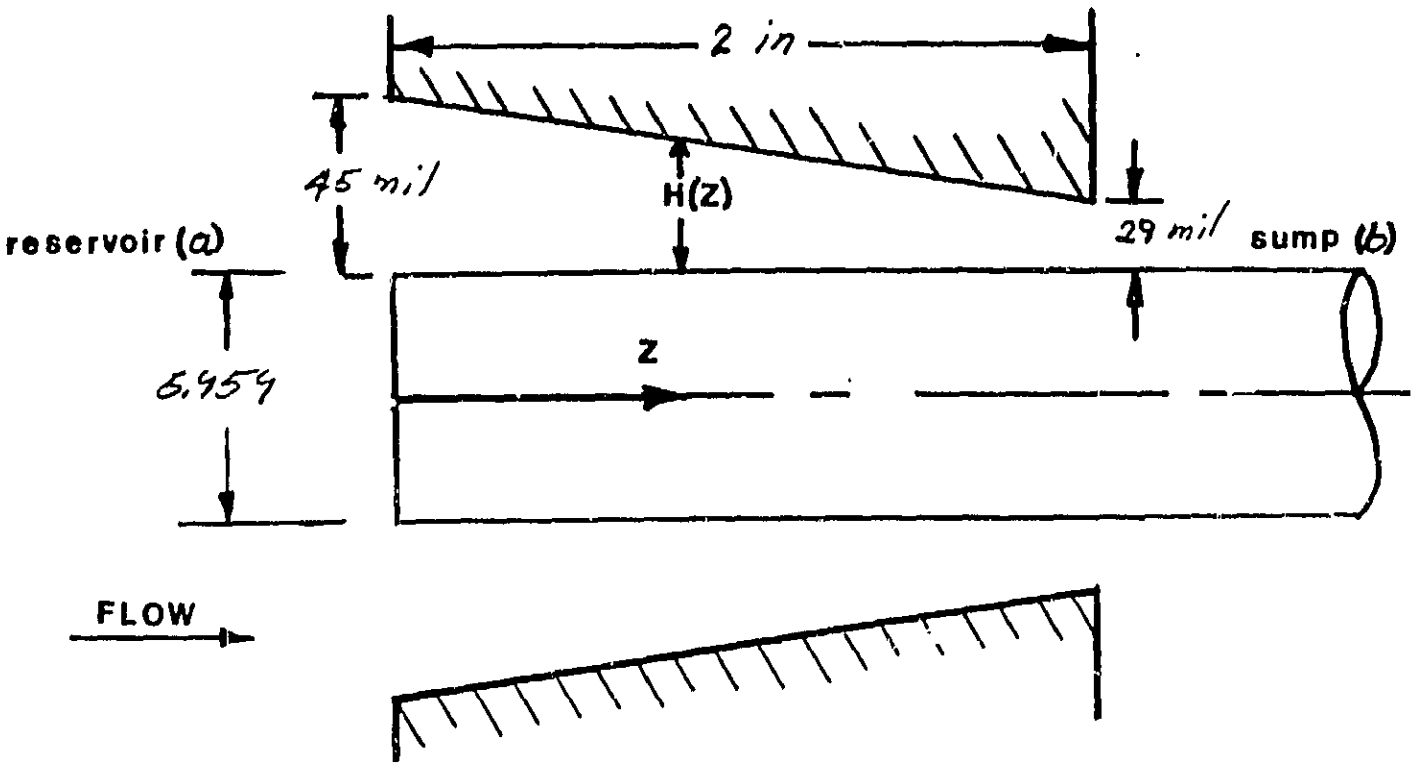

Figure 1 Geometry of the tapered annular seal.

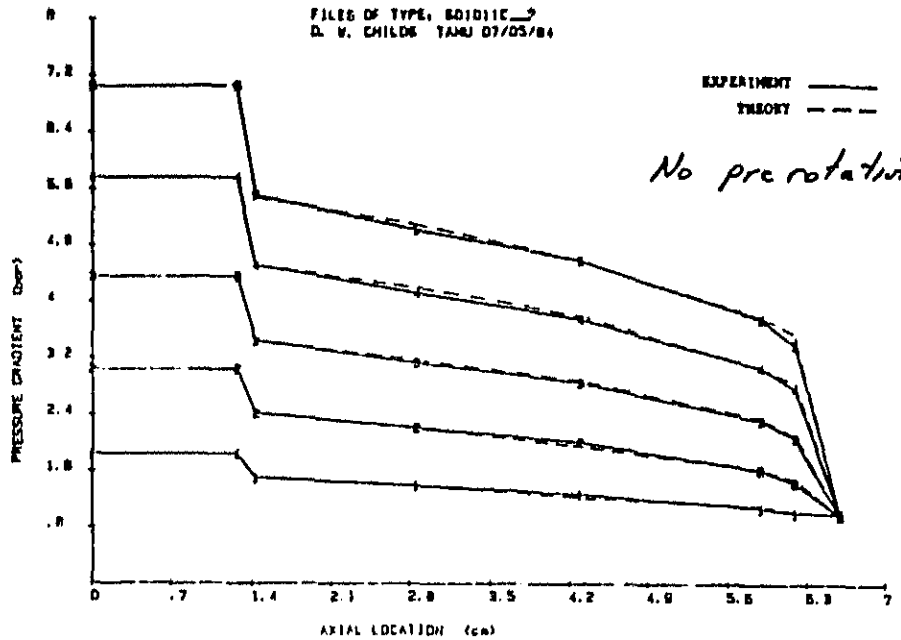

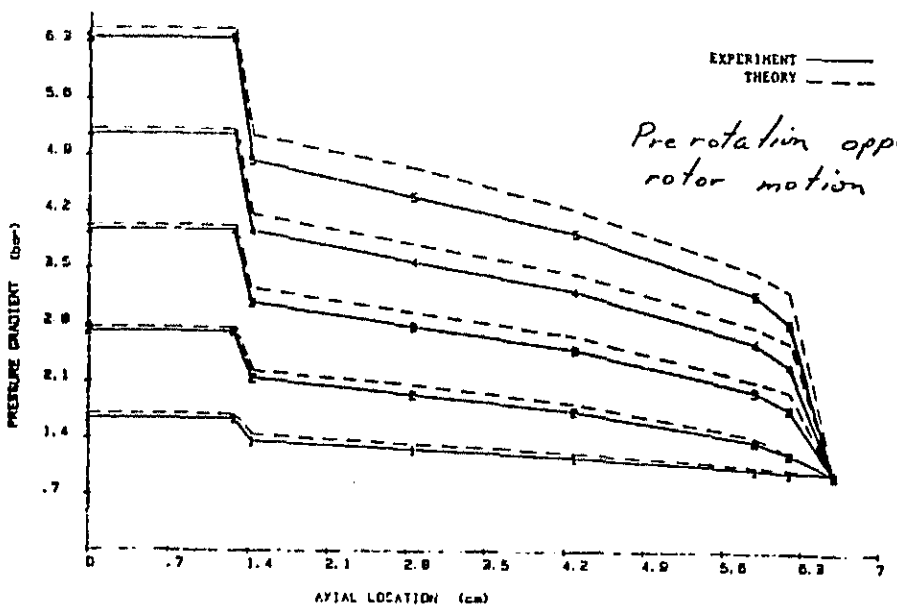

Fig. 2 Axial pressure gradient for the static test of the constant-clearance seal.

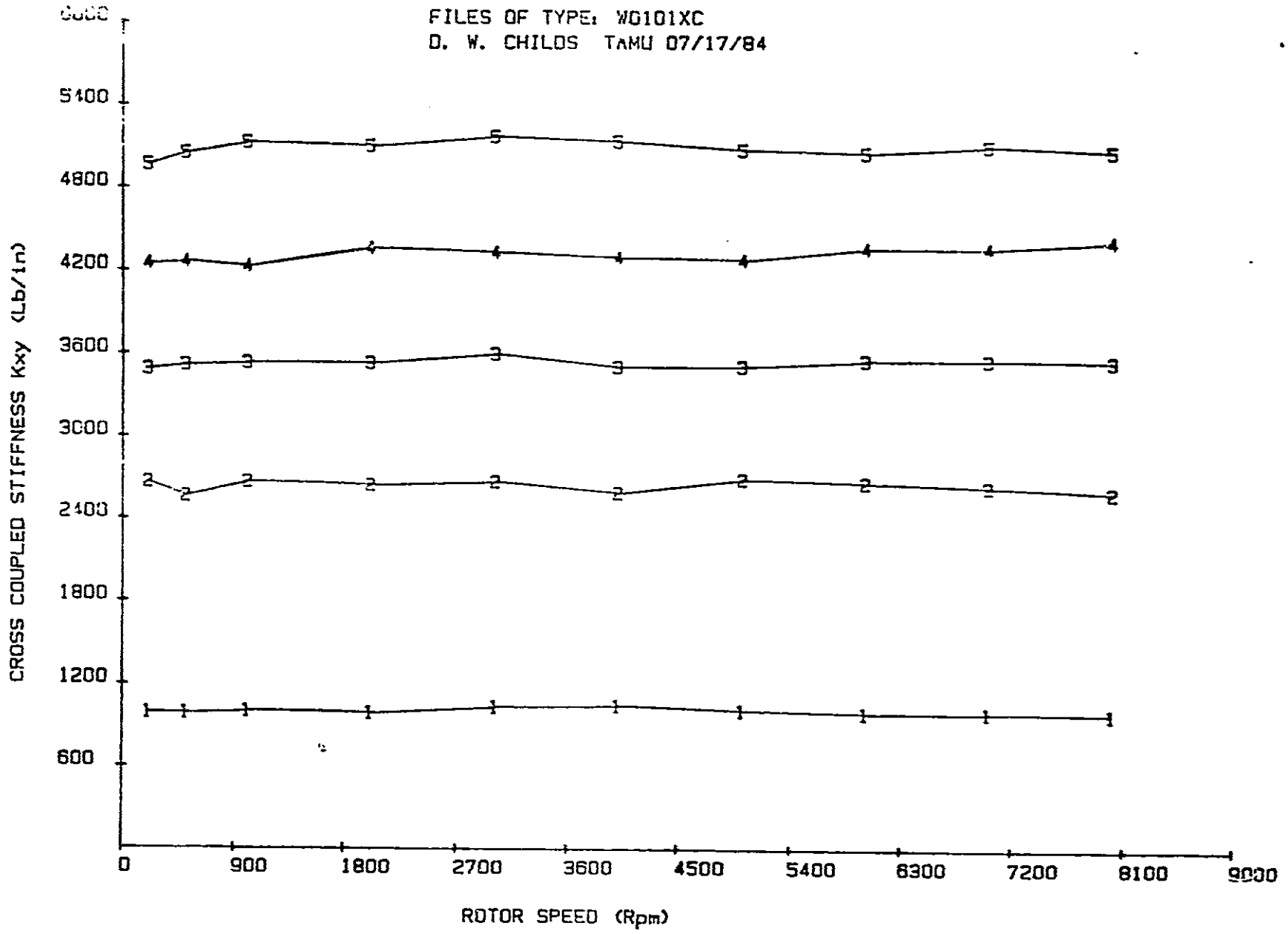

Fig. 3 Direct stiffness vs. rotor speed for the constant-clearance seal.

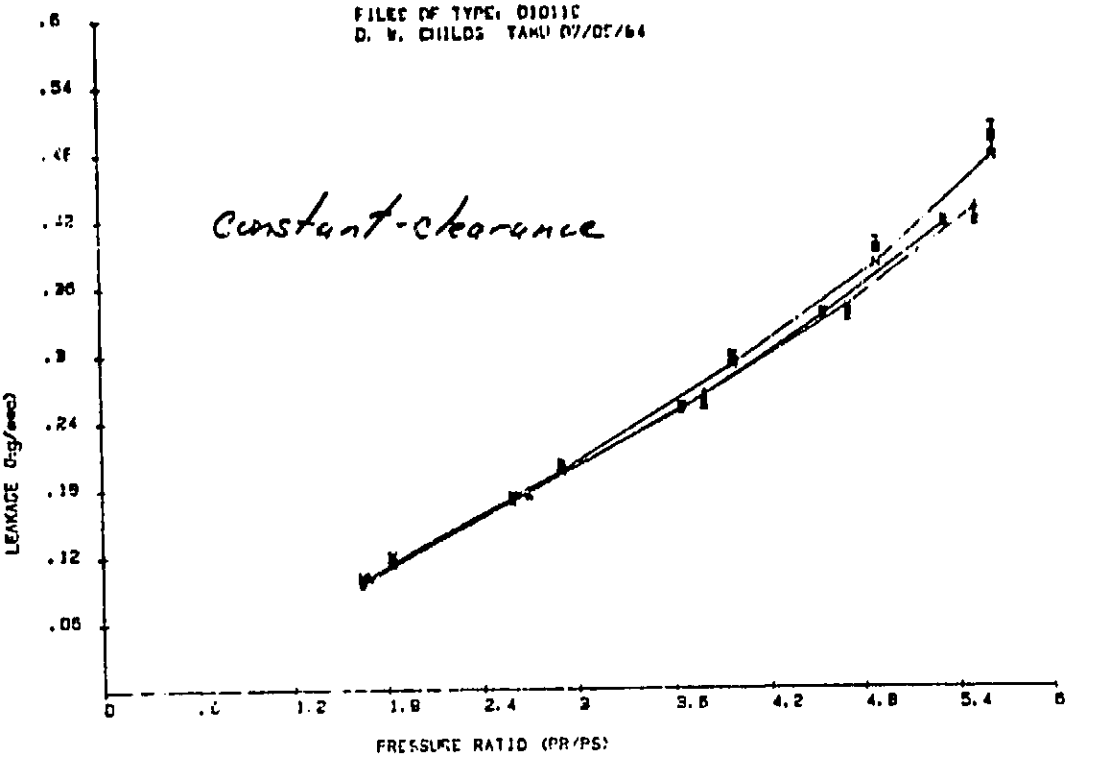

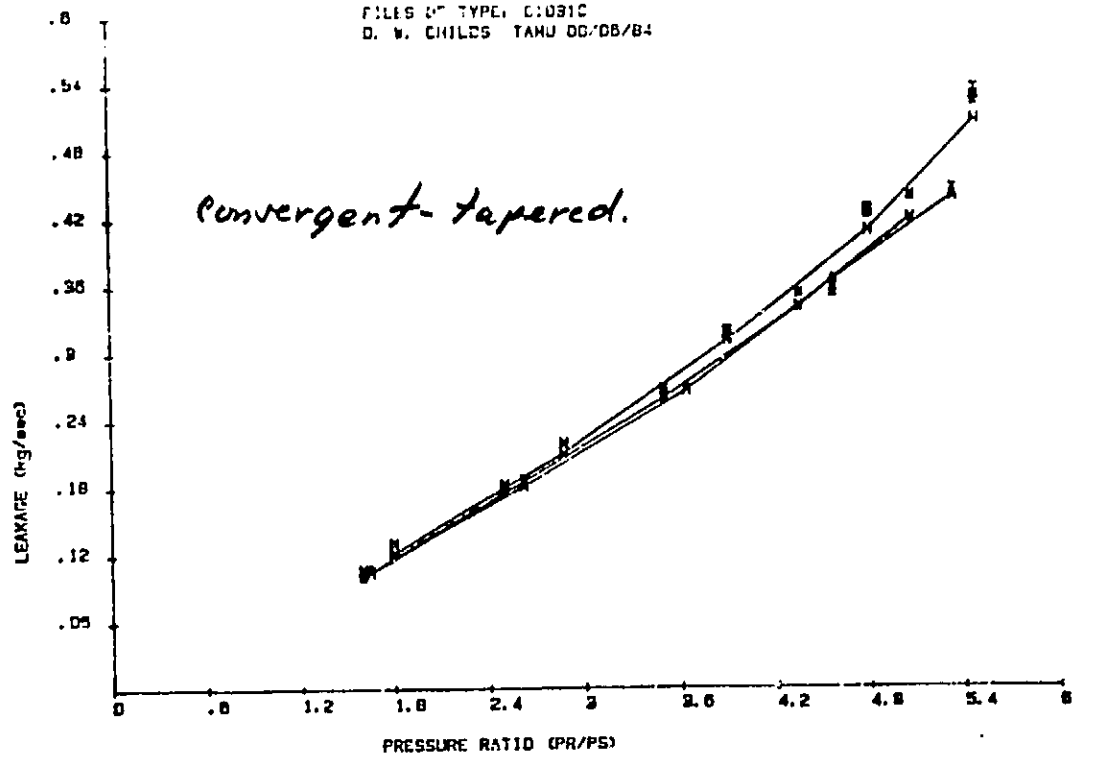

ORIGINAL PAGE IS
OE POOR QUALITY

Fig. 4 Leakage vs. pressure ratio ~~for the straight and tapered seal.~~

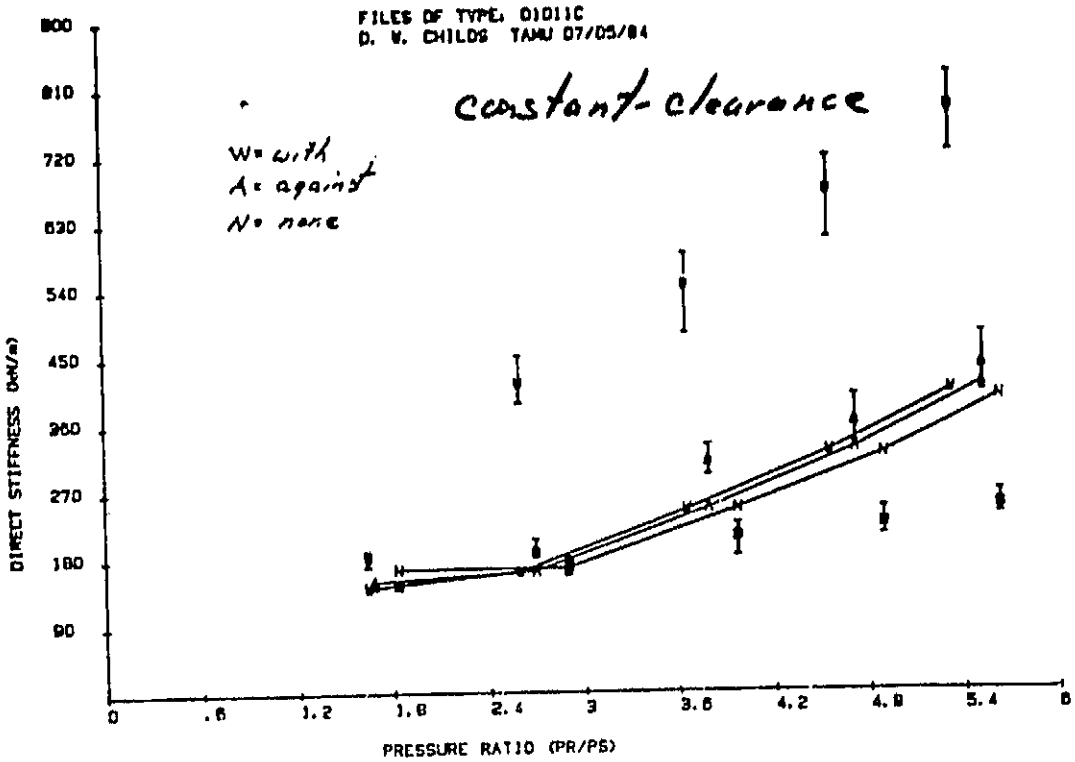

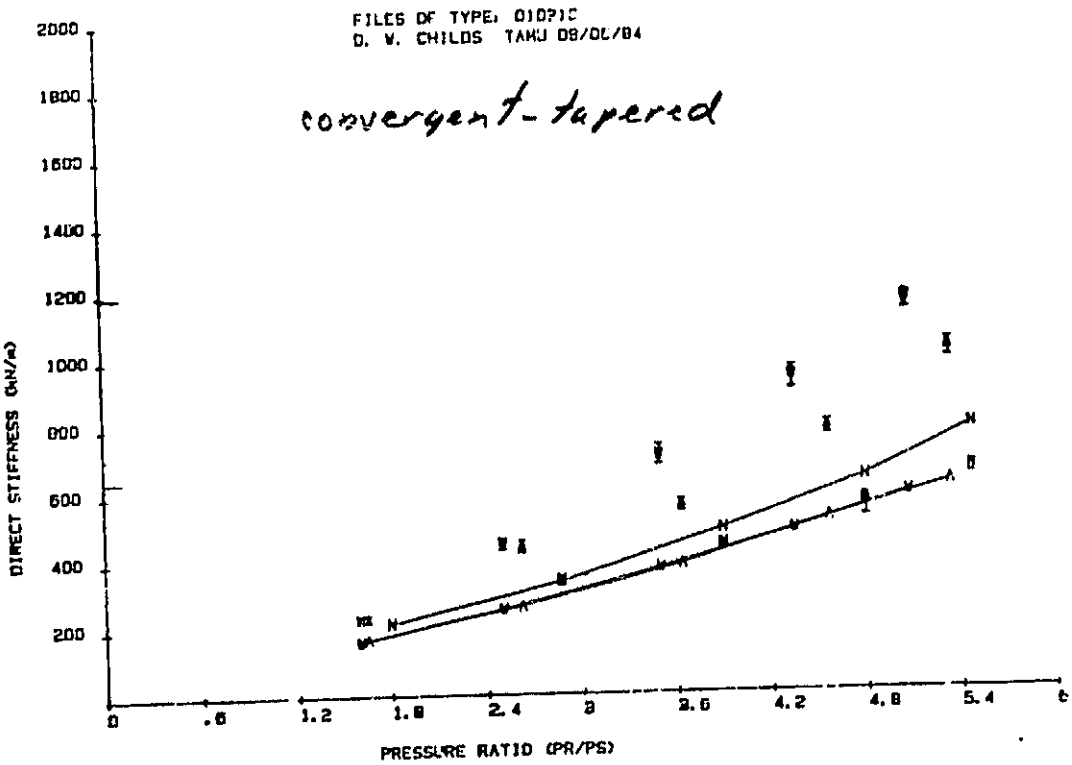

Fig 5 Direct stiffness vs. pressure ratio.

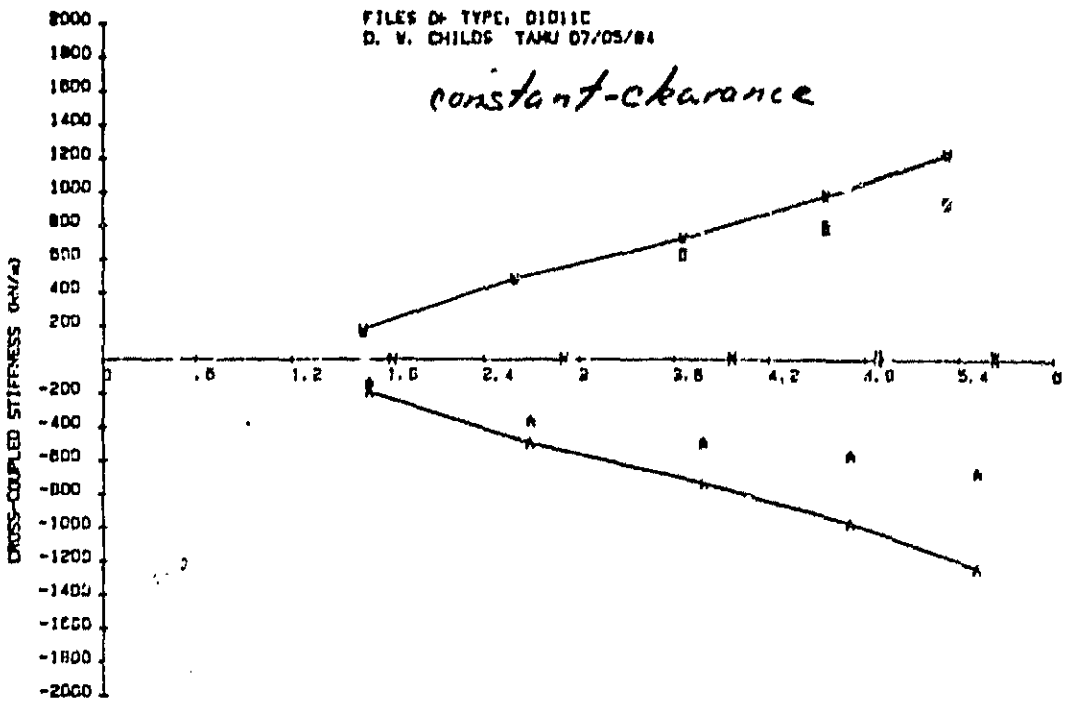

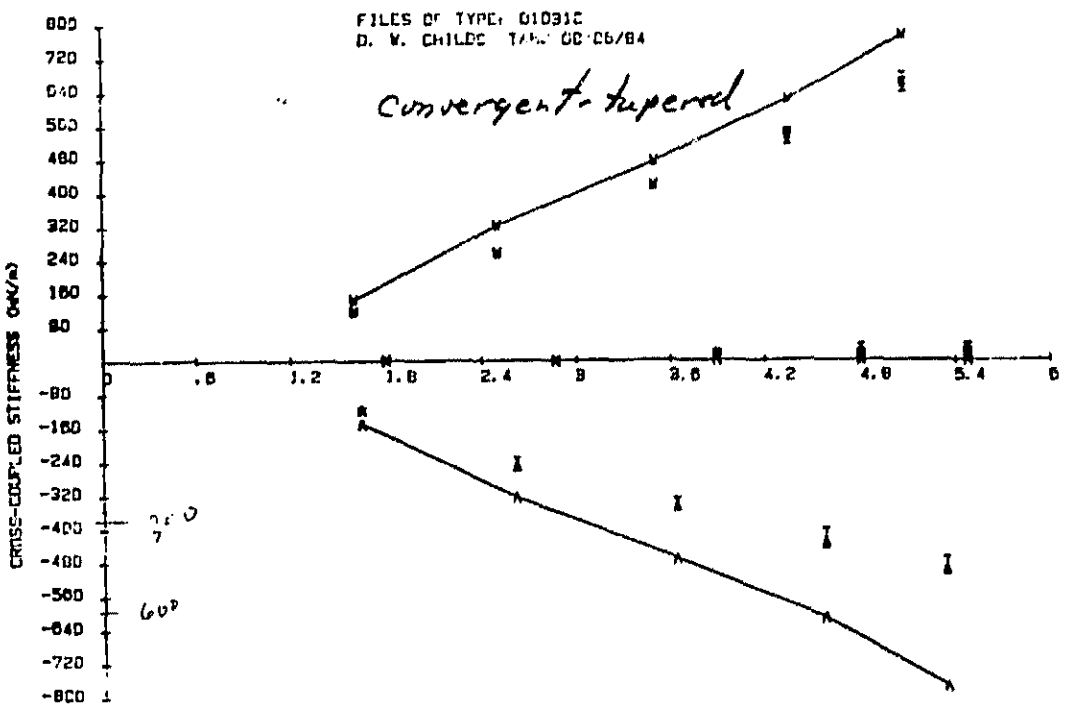

Fig. 6. Cross-coupled damping vs. pressure ratio

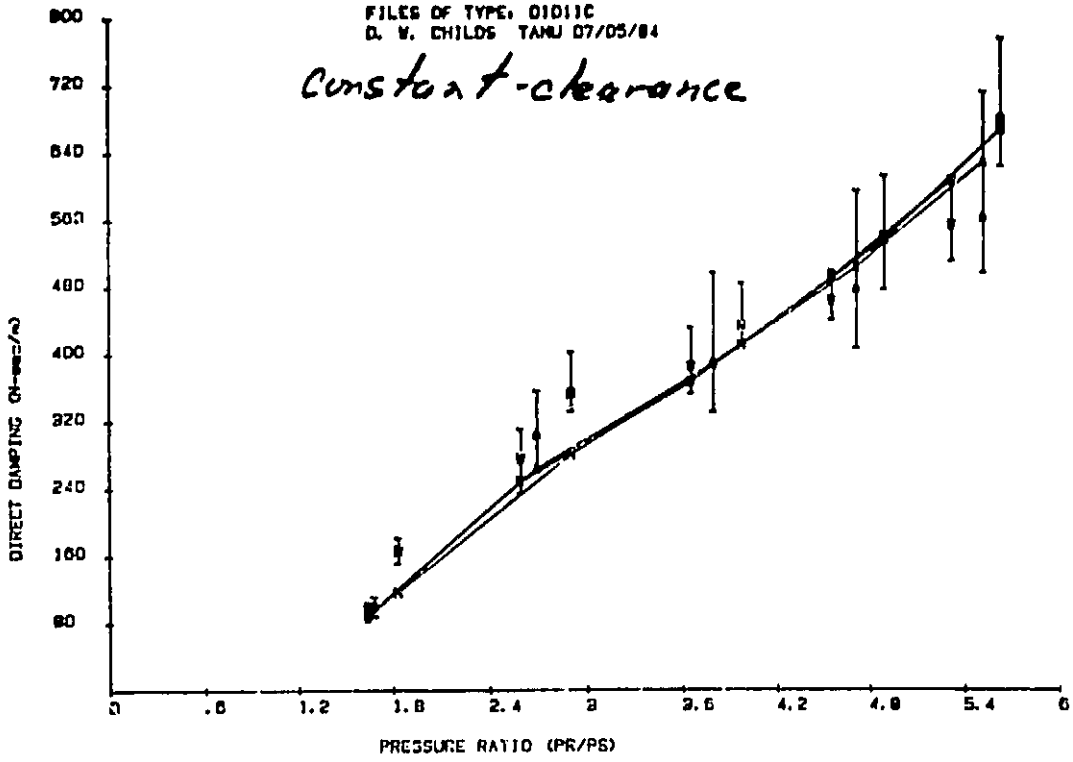

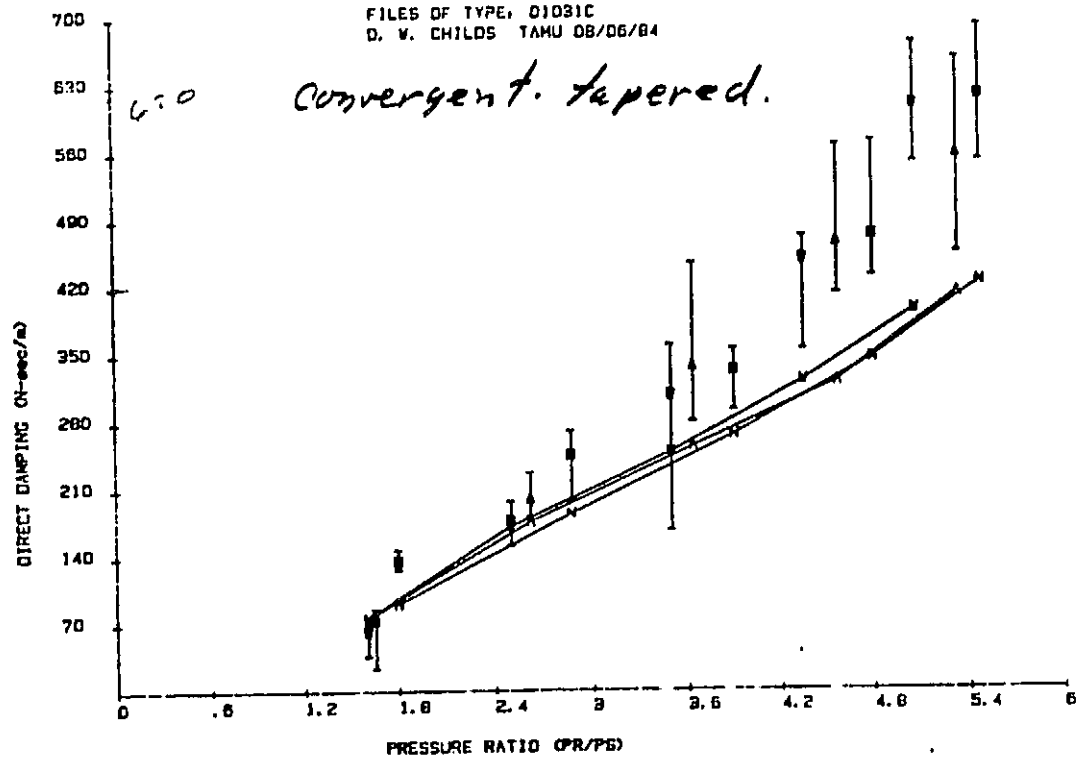

Fig. 7 Direct damping vs pressure ratio

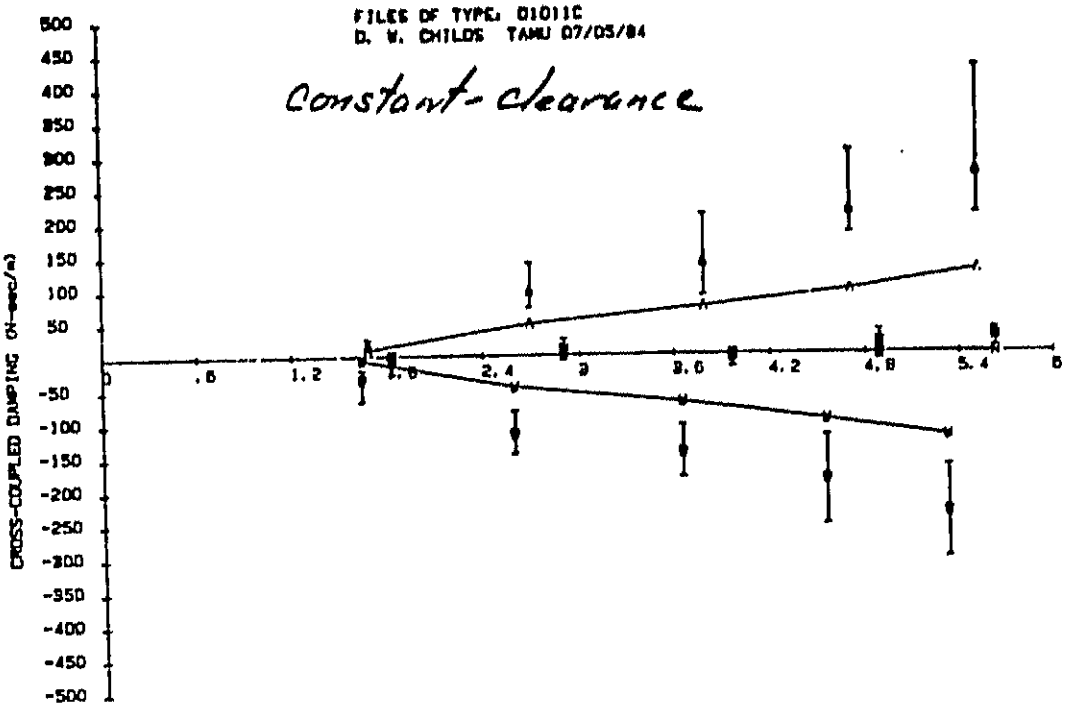

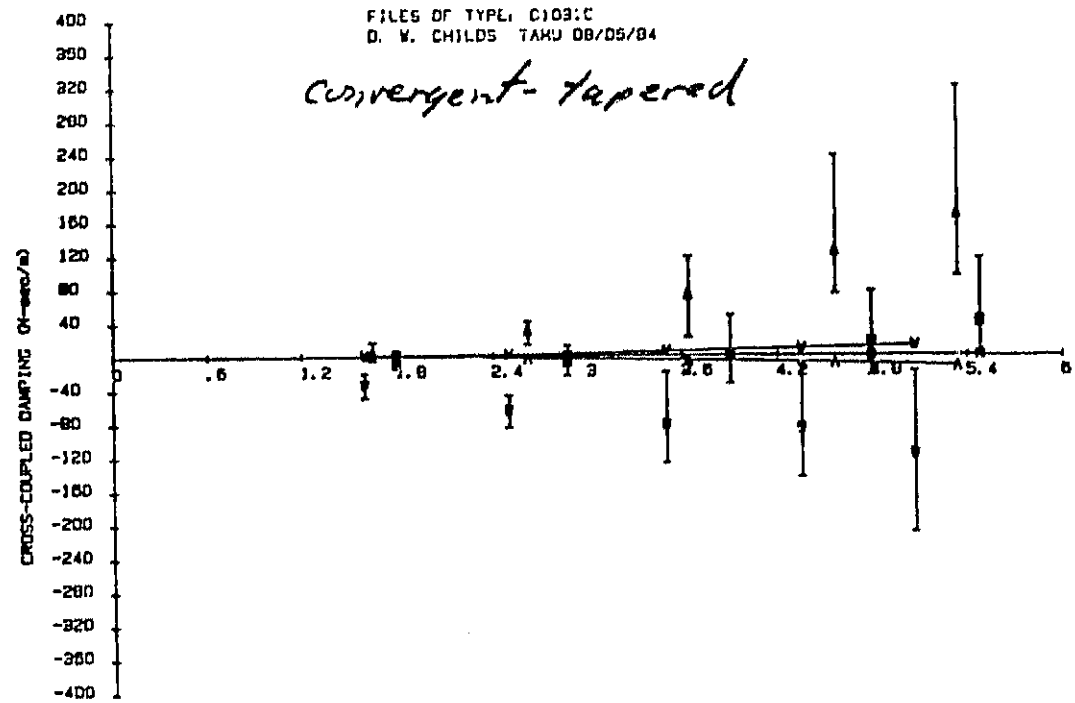

ORIGINAL PAGE IS
OF POOR QUALITY

Fig. 8 Cross-coupled damping vs. pressure ratio.

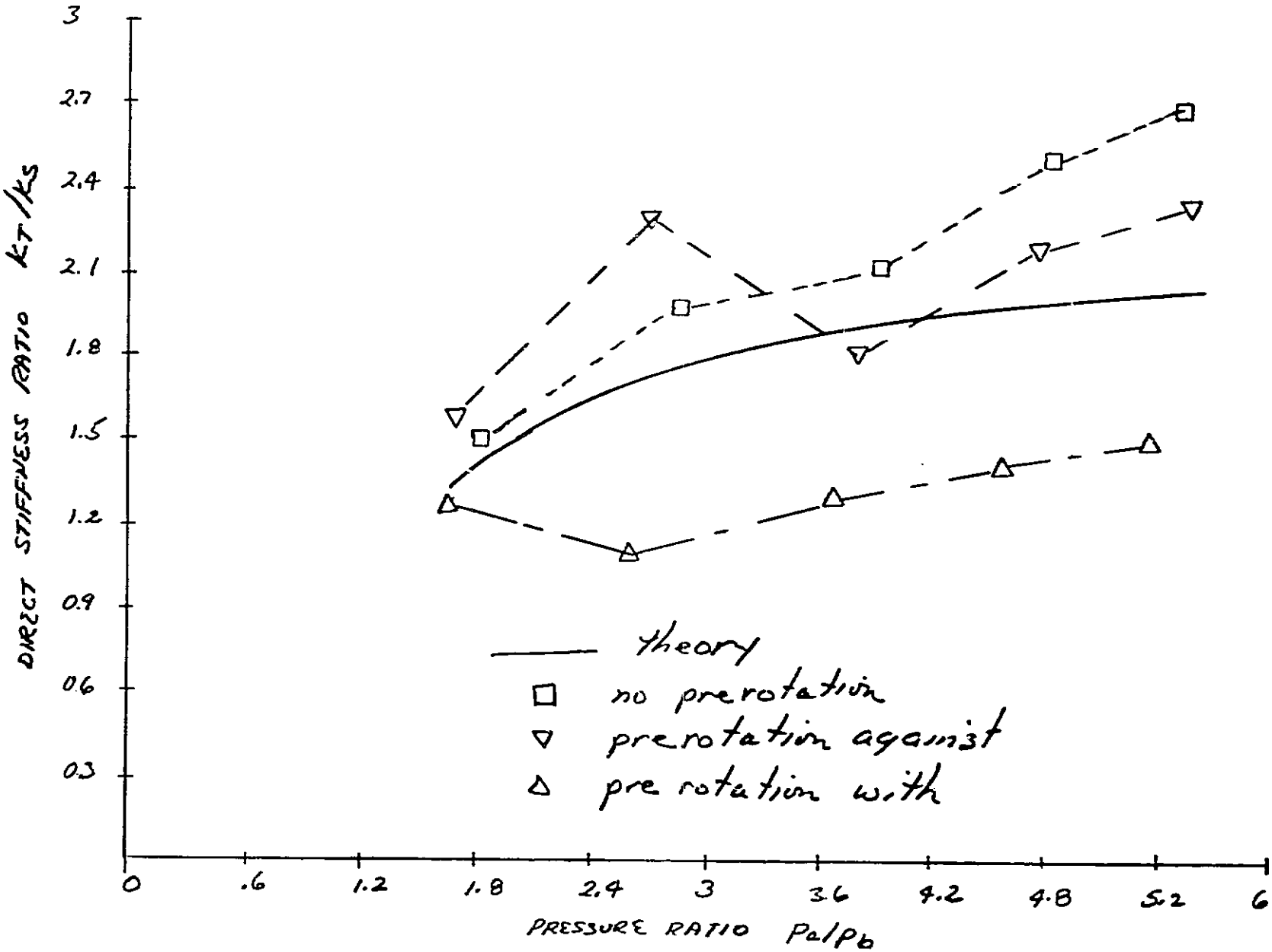

Fig. 9 Direct Stiffness ratio of the convergent-tapered and constant-clearance seal vs pressure ratio.